Charged Fuzzy Dark Matter Black Holes

Z. Yousaf,[1, *] Bander Almutairi,[2, †] S. Khan,[1, ‡] and Kazuharu Bamba[3, §]

[1]*Department of Mathematics, University of the Punjab, Lahore-54590, Pakistan.*
[2]*Department of Mathematics, College of Science,*
King Saud University, P.O.Box 2455 Riyadh 11451, Saudi Arabia
[3]*Faculty of Symbiotic Systems Science, Fukushima University, Fukushima 960-1296, Japan*

We investigate the impact of fuzzy dark matter (FDM) on supermassive black holes (SMBHs) characterized by a spherical charge distribution. This work introduces a new class of spherically symmetric, self-gravitational relativistic charged models for FDM haloes, using the Einasto density model. This study enables the dark matter (DM) to appear as the matter ingredient, which constructs the black hole and extends the non-commutative mini black hole stellar solutions. By considering the charged anisotropic energy-momentum tensor with an equation of state (EoS) $p_r = -\rho$, we explore various black hole solutions for different values of the Einasto index and mass parameter. Our approach suggests that the central density of the resulting black hole model mimics the usual de Sitter core. Furthermore, we discuss the possibility of constructing a charged self-gravitational droplet by replacing the above-mentioned EoS with a non-local one. However, under these circumstances, the radial pressure is observed to be negative. Ultimately, we consider various possibilities of constructing DM black holes, featuring intermediate masses that could evolve into galaxies. Consequently, some of these theoretical models have the potential to replace the usual black hole solutions of the galactic core. Simultaneously, these models are physically beneficial for being comprised of the fundamental matter component of the cosmos. Due to the outcomes of this paper, we would be able to study the connection between BH and DM by formulating stable stellar structures featuring fuzzy mass distributions derived from the Einasto distribution of DM halos.

PACS numbers:

I. INTRODUCTION

The relationship between astrophysical dark entities, such as black holes (BHs) and dark matter (DM), presents a fascinating and complex challenge in modern cosmology and astrophysics. Compact objects like BHs are cosmic vacuums where the gravitational field is highly dominant, opening new avenues for understanding the interaction between gravity and fundamental physics [1–3]. They originate from the collapse of massive stars or the merging of dense objects and have been thoroughly studied using Einstein's gravitational model. On the other hand, DM makes up about 27% of the total mass energy of the universe and remains an intriguing puzzle for researchers [4, 5]. Despite its pivotal influence in shaping large-scale cosmic structures, DM has not yet been directly observed. Different models have been suggested to explain the nature of DM, with the fuzzy dark matter (FDM) model emerging as a strong contender. The FDM model has attracted the attention of researchers due to its unique characteristics and implications for cosmic structures.

The FDM model is defined by its wave-like features, which stem from the quantum mechanical nature of light bosons with masses around 10^{-22} eV, including axions and other similar particles. The wave-like nature of FDM distinguishes it from other DM candidates, like cold DM, and has significant consequences for the structure and development of self-gravitating cosmic objects. Unique cosmic phenomena, such as interference patterns in density distributions, smooth cores in dark matter halos, and inhibited structure formation at small scales, are observed in FDM at both galactic and cosmic scales. These unique properties of FDM offer a fresh perspective on DM, particularly in regions of strong gravitational fields, like those near BHs. The motivation for exploring FDM in the context of BHs stems from the crucial role that DM, in any of its forms, plays in the dynamics of self-gravitational stellar systems. The existence of DM in close vicinity to BHs can affect their stability, evolution, and observable characteristics, including emission spectra, accretion processes, and gravitational wave signals. The distinctive quantum features associated with FDM further intensify its interaction with BHs, especially in regions of high density and intense curvature. The

*Electronic address: zeeshan.math@pu.edu.pk; Corresponding author
†Electronic address: baalmutairi@ksu.edu.sa
‡Electronic address: suraj.pu.edu.pk@gmail.com
§Electronic address: bamba@sss.fukushima-u.ac.jp

dynamics of matter and energy surrounding BHs can be affected by electromagnetic fields, which introduces another dimension to the study of BHs [6]. Electromagnetic radiation can interact with BHs, especially those that are charged or surrounded by magnetic fields [7–9]. A wide range of phenomena are produced by this interaction, including the production of relativistic jets, dynamics of the accretion disk, and energy extraction through the Penrose process. Under these conditions, FDM may alter the structure of the electromagnetic field and affect its behavior in ways that classical DM theories do not foresee [10, 11]. Studying this interaction is vital for understanding the observation data from BH systems. This data includes X-ray emissions, radio signals, and the recently detected gravitational wave signals resulting from BH mergers.

A key reason for exploring the fuzzy FDM model is its quantum mechanical properties. The existence of ultra-light bosonic particles in the FDM model produce wave-like characteristics on galactic scales. The "cusp-core" and "missing satellite" issues that are frequently encountered in cold DM simulations could be resolved by the FDM model by naturally smoothing out small-scale density fluctuations. Although observations have limited the FDM model, it remains a viable possibility. Certain astronomical data, such as the matter distribution in galactic halos and the rotation curves of dwarf galaxies, indicate that FDM might still be a good fit in some regimes. Based on the particular model under consideration, the limitations of the FDM model could alter when more accurate data become available. Other alternatives, such as mixed DM models or more complex FDM interactions, are still being explored, even if existing observations may rule out some parameter ranges (such as certain masses of FDM particles). There is still much to learn about the whole effect of FDM on the creation of stellar structures. Investigating the impact of ultralight scalar fields on gravitationally bound stellar structures could open up new directions in fundamental physics, including possibly relating DM to inflationary models in the early universe or string theory.

To acquire a better knowledge of the nature of BH, it is essential to explore their interior composition in more detail. This kind of study can be conducted from a geometric perspective [12–14]. Furthermore, understanding the type of matter that contributed to the BH's formation is equally essential for a comprehensive understanding [15, 16]. Since baryonic and leptonic matter makes up only 4% of the entire cosmic content, the density profiles of DM increase as we approach the galactic center, highlighting the importance of exploring the interplay between DM and BHs [17–19]. Since baryonic and leptonic matter makes up only 4% of the entire cosmic content, the density profiles of DM increase as we approach the galactic center, highlighting the importance of exploring the interplay between DM and BHs. The no-hair theorem generally prevents us from observing the interior attributes of BHs [20–22]. However, modeling the interior configuration of a BH, which is an established technique in the literature [23–25], has the potential to show whether a relationship between DM and BHs is possible. A recent effort in this direction was presented in [26–28], where the researchers model the central galactic object by assuming a DM profile that is fitted to the outer regions of the galaxy. Other potential relationships between the two key components of the galactic bulge were explored in the studies [29, 29] (and references therein), which further supports the idea that the BH plays a central role in galactic structure. Based on this scenario, we developed a new model of the central galactic object as a fuzzy BH or a self-gravitating compact droplet structure. This model is closely related to BH/droplet models inspired by non-commutative geometry [30], which feature a Gaussian matter distribution and a de Sitter equation of state (EoS). To successfully accomplish our objectives, we will couple the proposed density profile with a stress-energy tensor representing an anisotropic fluid and an EoS of the type $p_r = -\rho$. This form of EoS appears frequently in investigations of BHs [24, 25, 31, 32]. In this case, it produces different kinds of regular BH models. Before the possible existence of a supermassive BH at the heart of the Milky Way, known as Sagittarius A^*, various theoretical models were developed that replaced the central BH with other gravitational objects. Gravastars [33], boson stars [34], naked singularities [35], burning disks [35], quantum cores [36], and gravitationally bound clumps of DM based on the exponential-sphere density parameterizations [37] featured among them. Apart from the aforementioned endeavors, numerous other researchers have explored alternative mechanisms that could initiate the formation of SMBHs in the galactic centers. For example, the formation of traversable wormholes within the outer galactic halos based on Einasto parameterizations have been discussed in [38]. Also, the formation of DM wormholes using the NFW and King's density profiles have been examined in [39], while [40] investigated the evolution of topologically deformed DM wormholes subject to the Chaplygin gas EoS with different density functions. By using three different DM density functions, the influence of DM on the weak deflection angle by central galactic BHs has been analyzed in [41]. More recently, the authors of [42] constructed four different spherically symmetric BH models immersed into DM halos using the Generalized Uncertainty Principle, while the possible formation of BHs with DM halos dwarf galaxies is presented in [43]. Furthermore, the effect of DM on the quasinormal modes and quasibound states of SMBHs have been probed in [44]. The effect of FDM on SMBHs using spherical matter distribution has been explored in [45]. They showed that FDM establishes a soliton core that surrounds the SMBH at the galactic center. The spherically symmetric BHs based on pseudo-isothermal DM profile have been derived in [46].

On the other hand, the Einasto density model serves as a mathematical model employed to investigate the distribution of matter, including DM halos, around black holes. Retana-Montenegro et al. [47] studied different analytical features associated with the three-parameter Einasto density model and discussed the relevance of this DM halos

model in comparison to other density profiles. Numerous scientists have developed various black hole solutions by employing the Einasto density profile. Motivated by the prevalence of DM in galactic cores, Batic et al. [31] explored the effects of FDM on the supermassive stellar structures existing within the galactic structures. They investigated the possible formation of self-gravitational structures based on the FDM model, utilizing an anisotropic fluid distribution based on the Einasto density function. In their subsequent work [32], the same authors examined the feasibility of stable self-gravitational objects with fuzzy mass distribution motivated by standard DM density functions. These astronomical entities manifest in three forms: stable fuzzy self-gravitational droplets (non-horizon), and fuzzy BHs characterized by either one or two horizons. Figueiredo et al. [48] developed an asymptotically flat BH metric with anisotropic matter configuration using generic density models. These models exhibit several realistic astrophysical scenarios and can describe the galactic structures hosting SMBHs surrounding DM. Baes [49] presented a systematic approach to explore the dynamical and photometric structure of the range of Einasto models across the complete spectrum of model parameter space, in the context of DM halos.

This manuscript seeks to explore the combined effects of FDM and the electromagnetic field on BHs, focusing on their impact on the BH's properties and the surrounding spacetime geometry. Taking into account the wave-like character of the FDM model, we explore its quantum interference patterns and localized wave structures that interact with the gravitational and electromagnetic fields of the BH in the background of the Einasto density profile. These interactions are believed to impact important BH features such as accretion rates and energy output, which might be detected by astronomical data. The new features identified in this work might shed light on the mechanics of BHs and DM, which could lead to new possibilities for the indirect detection of FDM through astronomical measurements. The structure of this study is as follows: In the coming section, we define the Einasto density model and some associated definitions such as the mass function, lower incomplete Gamma function, and the density profile. In Sec. **III** and **IV**, we establish charged FDM structures subject to the de Sitter-type EoS, the corresponding effective potential their viability of regenerating the dynamics of stellar systems. Section **V** is devoted to constructing the self-gravitating fuzzy-charged DM composed of anisotropic fluid for the stable stats of massive particles, under the assumption of non-local EoS. Consequently, the conclusion follows at the end of the manuscript.

II.   THE EINASTO DENSITY MODEL

In 1965, Einasto [50] presented an alternative density model, which is generally used to study the distribution of cold DM halos in galaxy clusters. Einasto [51, 52] showed that the gravitational potential, mass density, and the cumulative mass profile are particular types of descriptive functions that are involved in the realistic modeling of the galactic system. These descriptive functions provide a faithful characterization of the system and are the fundamentals of the density function $\rho(r)$. Therefore, it is reasonable to assume the density configuration itself as the primary and fundamental descriptive function of a galactic model. This configuration should manifest the following characteristics

- Jump discontinuities should not be present in the above-mentioned descriptive functions.

- The density function $\rho(r)$ is a smooth and asymptotically zero. That is, $\rho(r) \in C^\infty(\mathbb{R}^+)$ with

$$\lim_{r \to \infty} \rho(r) = 0.$$

- $0 < \rho(r) < \infty \ \ \forall \ r > 0.$

- The system's total mass, effective radius, and central gravitational potential, all of which are linked to ρ, should have finite values.

Besides modeling different galaxies such as Sculptor dwarfs, M31, M32, M87, and Milky Way [51, 52], the Einasto DM model can also be used in describing the density of DM haloes [53–57]. Further, some analytical studies inspired by the Einasto DM model include the spherically symmetric galaxy (spiral and analytical) models, and their DM haloes characterized by the logarithmic slope have also been discussed in the literature [47, 58, 59]. Since the Einsato density model is generally considered in the simulation of Λ cold DM haloes [56, 57, 60], local DM density using galactic velocity curve [61], structural features of spiral as well as eliptical galaxies, bulges and bars using SDSS survey [62] and the properties of dwarf elliptical galaxies [63]. The Einasto model [51, 52] is characterized by the density function

$$\rho(r) = \rho_s \exp\left\{-d_\beta \left[\left(\frac{r}{r_s}\right)^{\frac{1}{\beta}} - 1\right]\right\}, \tag{1}$$

where r_s is the half-mass radius, d_β is the numerical constant controlling r_s, ρ_s denotes the central density at $r = r_s$ and β is the Einasto index. The Einasto density model can be parameterized in several ways as can be seen in the literature. However, one popular representation of the model for DM halos is defined by

$$\rho(r) = \rho_{-2} \exp\left\{ -2\beta \left[\left(\frac{r}{r_{-2}}\right)^{\frac{1}{\beta}} - 1 \right] \right\}. \tag{2}$$

Here, r_{-2} and ρ_{-2} denote the radius and density at which $\frac{d\ln\rho}{d\ln r} = -2$. Now, by assuming the scale length

$$h = \frac{r_{-2}}{(2\beta)^\beta} = \frac{r_s}{d_\beta^\beta}, \tag{3}$$

and the value of the charged central density

$$\rho_0 + e_0 = (\rho_s + e_s)\exp(d_\beta) = \rho_{-2}\exp(2\beta), \tag{4}$$

where e_s denotes the central charge. Furthermore, ρ_0 and e_0 denote the values of density and charge at $r = 0$. Using this value in Eq. (2), we get

$$\rho(r) = (\rho_0 + e_0)\exp\left[-\left(\frac{r}{h}\right)^{\frac{1}{\beta}} \right], \tag{5}$$

The charged DM density profile based on Einasto's parameterization consists of numerous components, each of which is dependent on its own four sets of parameters $\{\rho_0, \beta, h, e_0\}$. Therefore, it is possible to simulate a variety of stellar structures by giving certain values of parameters. For example, in the case of DM haloes with masses in the range of dwarf galaxies to rich galaxy clusters, $4.54 \lesssim \beta \lesssim 8.33$, where the average value of $\beta = 5.88$ [53]. It has been analyzed that the value of β decreases with redshift and mass, with $\beta \sim 4.35$ in the case of cluster-sized and $\beta \sim 5.88$ for galaxy-sized haloes in the Millennium Run [54]. Some analogous findings have been presented in the case of galaxy-sized haloes within the Aquarius simulations [64].

Next, we consider the following function

$$\gamma(\alpha, z) = \int_0^z \exp(-x)x^{\alpha-1}dx \quad (\text{Re } \alpha > 0), \tag{6}$$

which is the lower incomplete Gamma function. This expression results from the splitting of the complete Gamma function [65] $\Gamma(\alpha) = \int_0^\infty \exp(-x)x^{\alpha-1}dx$. Now, the total mass M of the Einasto parameterization with density function (5), can be written as

$$M = 4\pi(\rho_0 + e_0)\int_0^\infty x^2 \exp(-u)\,dx. \tag{7}$$

where $u = \left(\frac{r}{h}\right)^{\frac{1}{\beta}}$. The above expression can be rewritten as

$$M = 4\pi(\rho_0 + e_0)\beta\Gamma(3\beta), \quad \text{with} \quad \Gamma(3\beta) = \int_0^\infty \exp(-u)u^{3\beta-1}du. \tag{8}$$

Furthermore, the value of the density profile in terms of the total charged mass terms using Eq. (5), can be given as

$$\rho(r) = \frac{M}{4\pi\beta h^3 \Gamma(3\beta)} \exp\left[-\left(\frac{r}{h}\right)^{\frac{1}{\beta}} \right]. \tag{9}$$

III. MATTER DISTRIBUTION AND EINASTO'S DARK MATTER HALOS

In this section, we describe the formation of a BH solution endowed with spherical symmetry in the context of the Einasto density model. Furthermore, let M be the total mass of a gravitational object modeled by the density function (9), which reduces to the Gaussian distribution with $h = \sqrt{\theta}$ and $\beta = \frac{1}{2}$ studied in [11] for the derivation of non-commutative geometry motivated by Schwarzschild BH. We consider the most generic form of static, spherically symmetric metric as

$$ds^2 = g_{00}(r)dt^2 - g_{00}^{-1}(r)dr^2 - r^2 d\Omega^2, \tag{10}$$

with $d\Omega^2 \equiv d\theta^2 + \sin^2\theta d\varphi^2$. The total stress-energy tensor is considered to be the sum of two parts, M_η^μ and E_η^μ, for matter and electromagnetic interactions, respectively as

$$T_\eta^\mu = M_\eta^\mu + E_\eta^\mu. \tag{11}$$

The usual expression of stress-energy tensor for anisotropic matter distribution with density source (9) can be written in terms of a diagonal matrix as

$$M_\eta^\mu = \begin{pmatrix} \rho & 0 & 0 & 0 \\ 0 & -p_r & 0 & 0 \\ 0 & 0 & -p_\perp & 0 \\ 0 & 0 & 0 & -p_\perp \end{pmatrix}, \quad p_r \neq p_\perp. \tag{12}$$

Here, the functions ρ, p_r and $p_\perp$ denote the energy density, radial pressure, and tangential pressure, respectively. The electromagnetic contributions can be expressed by the following expression

$$E_\eta^\mu = -\frac{1}{4\pi}\left(F_{\eta\nu}F^{\mu\nu} - \frac{1}{4}\delta_\eta^\mu F_{\nu\sigma}F^{\nu\sigma}\right), \tag{13}$$

where $F_{\mu\eta}$ is the electromagnetic field tensor, which can be defined in terms of four potential $\mathcal{A}_\mu$ as

$$F_{\mu\eta} = \frac{\partial\mathcal{A}_\eta}{\partial x^\mu} - \frac{\partial\mathcal{A}_\mu}{\partial x^\eta}. \tag{14}$$

In the rest frame of reference, we adopt the gauge field $\mathcal{A}_\mu$ as

$$\mathcal{A}_\mu = (\phi(r), 0, 0, 0). \tag{15}$$

To determine the unknown metric coefficients appearing in Eq. (10), we consider the Einstein-Maxwell field equations, given as

$$R_\eta^\mu - \frac{1}{2}\mathbf{R}\delta_\eta^\mu = -8\pi T_\eta^\mu, \tag{16}$$

$$F_{\mu\eta;\nu} + F_{\eta\nu;\mu} + F_{\nu\mu;\eta} = 0, \tag{17}$$

$$F^{\mu\eta}_{;\eta} = -4\pi J^\mu. \tag{18}$$

where R_η^μ is the Ricci tensor, $\mathbf{R}$ is the Ricci scalar. It is important to note that we use the convention where fundamental constants like G (gravitational constant) and c (speed of light) are set equal to 1 (i.e., $G = c = 1$). Further, the current density J^μ is can be defined in terms of electric charge density $\sigma_e(r)$ as

$$J^\mu = \sigma_e(r)V^\mu, \tag{19}$$

where the four-velocity V^μ of the fluid is given as

$$V^\mu = \left(\frac{1}{\sqrt{g_{\mu\mu}}}, 0, 0, 0\right). \tag{20}$$

Then, combining Eq. (10) with Eqs. (18)-(20) provide the following differential equation

$$\frac{d^2\phi}{dr^2} + \frac{2}{r}\frac{d\phi}{dr} = \frac{4\pi\sigma_e}{\sqrt{g_{00}}}, \tag{21}$$

which is linear in ϕ. Solving the above differential equation, we get

$$\frac{d\phi}{dr} = \frac{q(r)}{r^2\sqrt{g_{00}}}, \tag{22}$$

where the total charge $q(r)$ is given as

$$\frac{d\phi}{dr} = \frac{q(r)}{r^2\sqrt{g_{00}}}, \quad \text{with} \quad q(r) = 4\pi\int_0^r \sigma_e(x)x^2 dx. \tag{23}$$

Here, $q(r)$ is the total charge enclosed by the spherically symmetric gravitational source. Thus the non-null constituents of M_η^μ are the four diagonal elements

$$E_0^0 = E_1^1 = -E_2^2 = -E_3^3 = \frac{q^2(r)}{8\pi r^4}. \tag{24}$$

Finally, the total stress-energy tensor for anisotropic charged matter distribution is given as

$$T_\eta^\mu = \begin{pmatrix} \rho + \frac{q^2}{8\pi r^4} & 0 & 0 & 0 \\ 0 & -p_r + \frac{q^2}{8\pi r^4} & 0 & 0 \\ 0 & 0 & -p_\perp - \frac{q^2}{8\pi r^4} & 0 \\ 0 & 0 & 0 & -p_\perp - \frac{q^2}{8\pi r^4} \end{pmatrix}, \tag{25}$$

where the total charge $q(r)$ and the electric field $\tilde{E}(r)$ are related by the formula

$$\frac{q^2(r)}{8\pi r^4} = \frac{\tilde{E}^2(r)}{8\pi}. \tag{26}$$

The Einstein-Maxwell field equations along with the conservation equation $\nabla_\mu T^{\mu\eta} = 0$, produces the anisotropic hydrostatic equilibrium equation (the Tolman-Oppenheimer-Volkov equation) for the electrostatic case as

$$\frac{dp_r}{dr} = -\frac{1}{2g_{00}} \frac{dg_{00}}{dr} (\rho + p_r) + \frac{2}{r} \left[\frac{q^2}{8\pi r^3} \frac{dq}{dr} - (p_r - p_\perp) \right], \tag{27}$$

where

$$\frac{1}{2g_{00}} \frac{dg_{00}}{dr} = \frac{4\pi r^4 p_r + mr - q^2}{r(r^2 - 2mr + q^2)}, \tag{28}$$

and the mass function $m(r)$ is

$$m = 4\pi \int_0^r \rho(x) x^2 dx + \int_0^r \frac{q(x)}{x} \frac{dq(x)}{dx} dx. \tag{29}$$

We can retrieve the standard form of Tolman-Oppenheimer-Volkoff equation by setting $q = 0$ in Eq.(27). In terms of the lower incomplete Gamma function, the gravitational mass $m(r)$ takes the form

$$m = \frac{M}{\Gamma(3\beta)} \gamma\left(3\beta, \left(\frac{r}{h}\right)^{\frac{1}{\beta}}\right) + \int_0^r \frac{q(x)}{x} \frac{dq(x)}{dx} dx. \tag{30}$$

We require that $T_0^0 = T_1^1 = -\rho(r)$. For this requirement, the source appears to be self-gravitational droplet with charged anisotropic fluid, whose radial and tangential pressures, respectively, are defined as

$$p_r(r) - \frac{q^2}{8\pi r^4} = -\left(\rho(r) + \frac{q^2}{8\pi r^4}\right) = \frac{M}{4\pi \beta h^3 \Gamma(3\beta)} \exp\left[-\left(\frac{r}{h}\right)^{\frac{1}{\beta}}\right]. \tag{31}$$

$$p_\perp + \frac{q^2}{8\pi r^4} = -\rho(r)\left[1 - \frac{1}{2\beta}\left(\frac{r}{h}\right)^{\frac{1}{\beta}}\right] - \frac{q^2}{8\pi r^3} \frac{dq}{dr}. \tag{32}$$

 The behavior of the radial (left panel) and tangential pressure (right panel) components is described in FIG 1. The most notable feature is the negative values of both the pressure components throughout the graph. This is a feature of exotic matter, which is commonly associated with gravitationally bound stellar objects. It is observed that p_r and $p_\perp$ exhibit maximum values near the horizon, while their values decrease as we move away from it. At large radial distances, the graphs converge asymptotically to 0, implying that the object's pressure gradually vanishes far from its core. By following this process, one can infer that the energy-momentum conservation equation is satisfied identically. Eventually, it is straightforward to show that Eq. (27) is trivially satisfied for the values of p_r and $p_\perp$ as provided by Eqs. (31) and (32), respectively. This technique implies that the Einasto density model characterizes
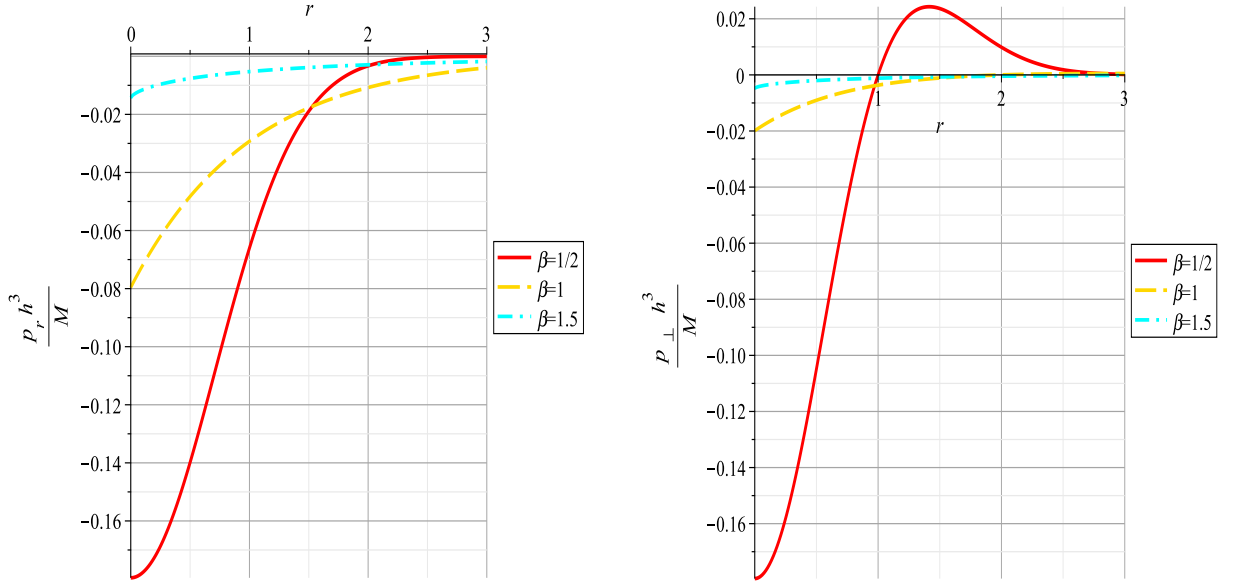
FIG. 1: Behaviors of $p_r h^3/M$ (on the left panel) and $p_\perp h^3/M$ (on the right panel) versus r/h with de Sitter-like EoS, $\rho = -p_r$. In case of DM, Einasto mass $M = 4.57 \times 10^9 M_\odot$, $h = 2.121 \times 10^{-9}$ kpc and the Einasto index $\beta = 0.7072$ [51, 52]. For normalized units $|p_r(0)| = |p_\perp(0)| \approx 5.8 \times 10^{-41} m^{-2}$ and in S.I units $|p_r(0)| = |p_\perp(0)| \approx 7 \times 10^3 N/m^2$. It is significant to understand that the tangential pressure alters its sign at $r_0 \approx 0.3$ kpc located within the active galactic nucleus [66].

an anisotropic self-gravitational fluid. Now by solving the Einstein-Maxwell field equations, with density profile (10), matter source(27), and the values of p_r and $p_\perp$, the line element turns out to be

$$ds^2 = \left(1 - \frac{2m}{r} + \frac{q^2}{r^2}\right) dt^2 - \left(1 - \frac{2m}{r} + \frac{q^2}{r^2}\right)^{-1} dr^2 - r^2 d\Omega^2, \tag{33}$$

or using expression (30), we get

$$ds^2 = \left(1 - \frac{2M}{r\Gamma(3\beta)}\gamma\left(3\beta, \left(\frac{r}{h}\right)^{\frac{1}{\beta}}\right) + \frac{q^2}{r^2} + \int_0^r \frac{q(x)}{x}\frac{dq(x)}{dx}dx\right) dt^2 - \left(1 - \frac{2M}{r\Gamma(3\beta)}\gamma\left(3\beta, \left(\frac{r}{h}\right)^{\frac{1}{\beta}}\right) + \frac{q^2}{r^2}\right.$$
$$\left. + \int_0^r \frac{q(x)}{x}\frac{dq(x)}{dx}dx\right)^{-1} dr^2 - r^2 d\Omega^2, \tag{34}$$

where

$$g_{00}(r) = 1 + \left(\frac{q}{r}\right)^2 - \frac{2M}{r\Gamma(3\beta)}\gamma\left(3\beta, \left(\frac{r}{h}\right)^{\frac{1}{\beta}}\right) + \int_0^r \frac{q(x)}{x}\frac{dq(x)}{dx}dx. \tag{35}$$

Here, it is significant to note that the metric (34) reduces to the classical Reissner-Nordström line element in the limit $\frac{r}{h} \to \infty$. Moreover, by assuming the metric coefficient g_{00} as a function of $\frac{r}{h}$ and introducing the rescaled mass $\omega := \frac{M}{h}$, there must exists a value of ω, say, ω_0, such that g_{00} has a double root at $u_0 := \frac{r_0}{h}$. Furthermore, two distinct event horizons exist for $\omega > \omega_0$ and no horizon for $0 < \omega < \omega_0$. Additionally, the behavior of the relativistic metric potential g_{00} may be realized by using the relation (see [67] for details)

$$\gamma(a, z) = z^{-a}\gamma^*(a, z)\Gamma(a, z), \quad \text{with} \quad \gamma^*(a, z) = \exp(-z)\sum_{n=0}^{\infty}\frac{z^n}{\Gamma(a+n+1)}. \tag{36}$$

The metric function $g_{00}(r)$ turns out to be

$$g_{00}(r) = 1 + \left(\frac{q}{r}\right)^2 - 2\omega\left(\frac{r}{h}\right)^2\exp\left[-\left(\frac{r}{h}\right)^{\frac{1}{\beta}}\right]\sum_{n=0}^{\infty}\frac{\left(\frac{r}{h}\right)^{\frac{n}{\beta}}}{\Gamma(3\beta+n+1)} + \int_0^r \frac{q(x)}{x}\frac{dq(x)}{dx}dx. \tag{37}$$
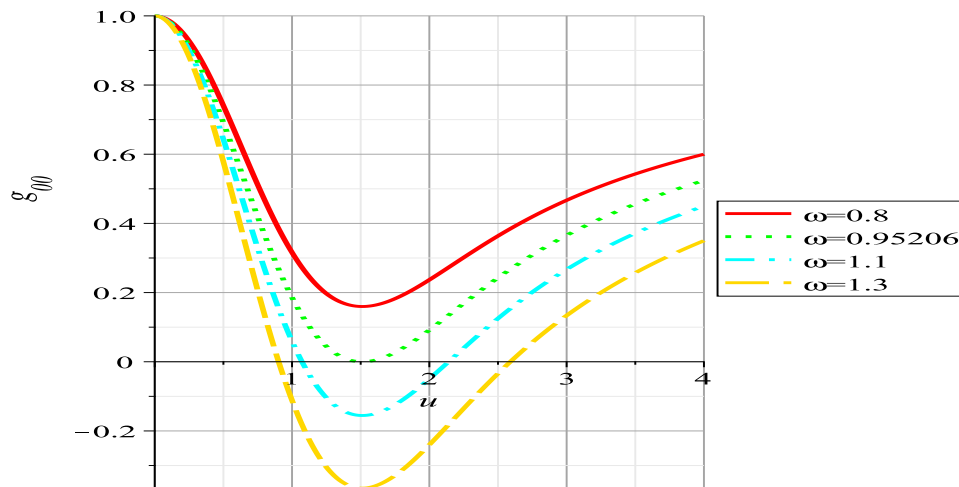
FIG. 2: Behavior of the relativistic metric potential g_{00} versus $u := (\frac{r}{h})^{1/\beta}$ with Einasto index $\beta = 0.5$ for different values of the rescaled parameter ω.

The above-mentioned expression behaves alternatively, as in the case of Reissner-Nordström BH and the Schwarzschild BH, where singularity appears at $r = 0$. In this case, a standard de Sitter core is used to characterize the central region. Consequently, one can deduce that Einasto's density model with anisotropic energy-momentum tensor for an EoS $p_r = -\rho$, solves the problem of central density. Furthermore, there is no naked singularity as well as no event horizon for the case $\omega < \omega_0$. FIG. 2 shows the variation of the metric function subject to the Einasto density model. The metric function assumes a negative values, a typical feature of a gravitational field. This shows that the object has a gravitational attraction on the nearby test particles. The radii of the event horizons in terms of the variable u are characterized by the intersections on the u-axis. There is only one degenerate horizon for $\omega_0 = 2.28378$ with $\omega = \omega_0 = 0.95206$. The value $\omega_= 0.8 < \omega_0$ corresponds to no horizon case, whereas $\omega = 1.1 > \omega_0$ corresponds to two horizons. Notable, the former case represents the self-gravitational droplet coupled with anisotropic stress energy tensor. Let us now calculate the Hawking temperature $T_{\mathcal{H}}$ for this novel class of BHs by using the formula [11] as

$$T_{\mathcal{H}} = \frac{1}{4\pi}\left(\frac{dg_{00}}{dr}\right)_{r=r_{\mathcal{H}}} = \frac{2q}{r_{\mathcal{H}}^2}\left(\frac{dq}{dr} - \frac{q}{r_{\mathcal{H}}}\right) + \frac{1}{4\pi r_{\mathcal{H}}}\left\{1 - \frac{r_{\mathcal{H}}^3 \exp\left[-\left(\frac{r}{h}\right)^{\frac{1}{\beta}}\right]}{h^3\beta\gamma(3\beta, \left(\frac{r}{h}\right)^{\frac{1}{\beta}})}\right\} + \frac{q}{r_{\mathcal{H}}}\frac{dq}{dr_{\mathcal{H}}}, \tag{38}$$

where M and $r_{\mathcal{H}}$ are the total mass and the position of the event horizon, respectively. We can obtain the eventual event horizon by using the expression $g_{00}(r_{\mathcal{H}}) = 0$, that is

$$r_{\mathcal{H}} = 2m - \frac{q^2}{r} = \frac{2M}{r\Gamma(3\beta)}\gamma\left(3\beta, \left(\frac{r}{h}\right)^{\frac{1}{\beta}}\right) - \frac{q^2}{r} - \frac{1}{r}\int_0^r \frac{q(x)}{x}\frac{dq(x)}{dx}. \tag{39}$$

It is notable that the expression (38) reduces to the classical result $T_{\mathcal{H}} = (4\pi r_{\mathcal{H}})^{-1}$ for the case $\frac{r_{\mathcal{H}}}{h} \gg 1$ and $q = 0$.

IV. THE EFFECTIVE POTENTIAL

This section aims to figure out whether the diffuse BH models comprised of DM, presented in the previous section, can be consistent with the model of central galactic BH with mass $M_{BH} = 4.1 \times 10^{-6}M_{\odot}$ and Schwarzschild radius $R_{BH} = 2G_N M_{BH}/c^2 = 17.4\,R_{\odot} = 3.92 \times 10^{-7}$ pc. For this, we need to understand the relevant parameters, i.e., the Einasto index β and the rescaling factor h in the considered model. More specifically, this can be completed in two ways. Firstly, by imposing the condition that the total mass M appearing in the geometry (34) coincides with M_{BH}. Nextly, when measured at the r_{min} of the effective potential associated with a massive particle, the mass m offers an accurate estimation for M_{BH}. Alternatively, we require that

$$1 - \frac{m(r_{min})}{M_{BH}} \leq 10^{-2}. \tag{40}$$

This expression can be rewritten in an equivalent form by using Eq. (29) as

$$\Delta\gamma \equiv \frac{1}{\Gamma(3\beta)}\gamma\left(3\beta, \left(\frac{r_{min}}{h}\right)^{\frac{1}{\beta}}\right) - 0.99 \geq 0, \tag{41}$$

It turns out that the aforementioned criterion not only guarantees the equivalence between our diffused self-gravitating structure and the Schwarzschild effective potential at their minimum but they both also coincide within a substantial range of it as well as in the far limit. The effective potential U^{eff} for this investigation is calculated by using the geodesic equation of motion. Particularly, by employing the method as discussed in [68], we can transform the radial equation into an energy-conservation equation given as

$$\frac{dr}{d\tau} + U^{\text{eff}}(r) = constant, \tag{42}$$

where τ denotes the proper time, which depends on whether a massless or heavy particle is assumed. Therefore, the effective potential corresponding to the spherical metric characterized by the ansatz (10) is given as [68]

$$U^{\text{eff}} = \frac{\ell}{2r^2}\left(1 - \frac{2m}{r} + \frac{q^2}{r^2}\right) - \xi\frac{m}{r}, \quad \text{where} \quad \xi = \begin{cases} +1 & \text{if } m_p \neq 0 \\ -1 & \text{if } m_p = 0 \end{cases}, \tag{43}$$

with ℓ and m_p represent the total angular momentum per unit mass and the mass of a test particle, respectively. We can express the above relation using Eq. (6) as

$$U^{\text{eff}} = \frac{\ell^2}{2r^2} - \frac{M_{BH}}{\Gamma(3\beta)}\gamma\left(3\beta, \left(\frac{r}{h}\right)^2\right)\left(\frac{\xi}{r} + \frac{\ell^2}{r^2}\right) + \frac{\ell^2 q^2}{2r^4}. \tag{44}$$

Notably, the effective potential for the Schwarzschild case can be written as

$$U_S^{\text{eff}} = \frac{\ell^2}{2r^2} - M_{BH}\left(\frac{\ell^2}{r^2} + \frac{\xi}{r}\right). \tag{45}$$

Let us take $r_s = 2M_{BH}$ and consider a rescaling of the variables ℓ and r such that $\mathscr{L} = \frac{\ell}{r_s}$ and $r^* = \frac{r}{r_s}$. Thus for the massive case, the Schwarzschild effective potential may take the following form

$$U_S^{\text{eff}} = -\frac{1}{2r^*} + \frac{\mathscr{L}^2}{2r^{*2}}\left(1 - \frac{1}{r^*}\right), \tag{46}$$

where $r^* = 1$ is defined as the location for the gravitational event horizon. In addition, the maximum and minimum values of r^* are given as

$$r_{min}^* = \frac{\mathscr{L}^2}{2}\left(1 + \sqrt{1 - \frac{3}{\mathscr{L}^2}}\right), \quad r_{max}^* = \frac{\mathscr{L}^2}{2}\left(1 + \sqrt{1 - \frac{3}{\mathscr{L}^2}}\right) \quad \text{with} \quad \mathscr{L} > \sqrt{3}, \tag{47}$$

respectively. After introducing the above-mentioned rescaling for ℓ and r in Eq. (43), we obtain

$$U^{\text{eff}} = \frac{\mathscr{L}^2}{2r^2} - \frac{1}{\Gamma(3\beta)}\gamma\left(3\beta, \left(\frac{r^*}{\mathcal{H}}\right)\right)\left(\frac{1}{2r^{*2}} + \frac{\mathscr{L}^2}{2r^{*3}}\right) \quad \text{with} \quad \mathcal{H} = \frac{h}{r_s}, \tag{48}$$

and

$$\Delta\gamma \equiv \frac{1}{\Gamma(3\beta)}\gamma\left(3\beta, \left(\frac{r_{min}^*}{\mathcal{H}}\right)\right) - 0.99 \geq 0. \tag{49}$$

This constraint represents an inequality in the Einasto index β and the parameter $\mathcal{H}$. To display that the solution set obtained from this is non-empty, we will analyze certain values of the parameter $\mathcal{H}$ to ensure the similar magnitude orders of the associated parameter $h = r_s\mathcal{H}$ as in [51, 52, 61]. We can solve (49) by considering different values of the $\mathcal{H}$ with respect to the Einasto index β. The above-mentioned approach implies that we need to fix the value of total angular momentum $\mathscr{L}$ because the specific value of r_{min}^* depends on $\mathscr{L}$. For example, the value of the rescaled parameter $h_E = 2.121 \times 10^{-9}$ kpc in the case of DM haloes [51, 52]. Therefore, the value of the rescaled parameter in our case is $h = 3.92 \times 10^{-9}$ kpc corresponding to $\mathcal{H} = 10$. We explore several choices of $\mathscr{L}$ and r_{min}^* to determine
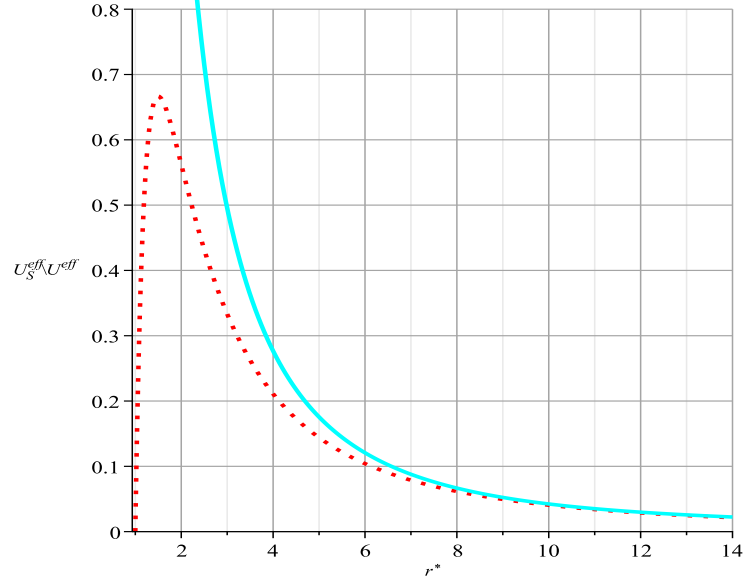
FIG. 3: Pictorial representation of the effective potentials U_S^{eff} (dotted line) and U^{eff} (solid) with $\beta = 0.2$, $\mathscr{L} = 3$ and $\mathcal{H} = 10$ for the massless case. For this value of $\mathcal{H}$, the central galactic system is modeled as an anisotropic self-gravitational droplet with scaling factor h of the order $h_E = 2.21 \times 10^{-9}$kpc [51, 52]. Significantly, the Schwarzschild BH's event horizon is located at r^*, whereas the maximum value of U_S^{eff} is positioned at the photon sphere radius $r_\gamma^* = 3/2$. The self-gravitational droplet does not contain the photon sphere because U^{eff} fails to display a maximum value.

which values will fulfill Eq. (49). We notice that the expression (49) cannot be fulfilled with $r_{min}^* = 6$ and $\mathscr{L} = 2$ because in this case, numerical results show that $\Delta\gamma < 0$ within the range $10^{-6} \leq \beta \leq 13$ [31]. To address the issue that whether the presented solution characterizes a fuzzy droplet or the fuzzy BH model with $\mathcal{H} = 10$ and considered β so that Eq. (49) is fulfilled, we observe that $r_s = 2M_{BH}$ implies $M_{BH} = \frac{r_s}{2}$ in case of geometric units and the rescaling mass parameter ω for our model can be defined as

$$\omega = \frac{1}{2\mathcal{H}} = \frac{M_{BH}}{h} = \frac{r_s}{2h} \quad \text{where} \quad h = r_s\mathcal{H}. \tag{50}$$

The behavior of effective potential for the Schwarzschild case and the diffused compact droplet with different values of $\mathcal{H}$, for the massless case, is illustrated in FIGs. 3 and 4. The profiles show that both the Schwarzschild effective potential and the effective potential of our diffused self-gravitational structure have the same photon sphere, and they coincide over a significant range and at asymptotically large distances. Furthermore, by introducing the rescaling $r^* = \frac{r}{r_s}$ and $Q = \frac{q}{r_s}$ in expression (37), the value of g_{00} takes the form

$$g_{00} = 1 + \left(\frac{Q}{r^*}\right)^2 - 2\omega \left(\frac{r^*}{\mathcal{H}}\right)^2 \exp\left[-\left(\frac{r^*}{\mathcal{H}}\right)^{\frac{1}{\beta}}\right] \sum_{n=0}^{\infty} \frac{\left(\frac{r^*}{\mathcal{H}}\right)^{\frac{n}{\beta}}}{\Gamma(3\beta + n + 1)} + \int_0^{r^*} \frac{Q(x)}{x} \frac{dQ(x)}{dx}. \tag{51}$$

FIG. 5 reveals that the equation $g_{00}(r^*)$ has no real roots. This shows that this model predicts a fuzzy self-gravitating droplet. A closer look at FIG. 6 suggests that, unlike in the case when $\mathcal{H} = 10$, we have a more complex scenario. If β is less than 1.2865, so we get a BH composed of DM with two horizons. If β is higher than 1.2865, we observe a diffuse DM droplet without a horizon. This same scenario occurs if we lower the value of $\mathcal{H}$ even further. The behavior of effective potential for the Schwarzschild case and the diffused compact droplet with different values of $\mathcal{H}$ for the massive case is illustrated in FIGs. 7. This shows that the Schwarzschild effective potential and the effective potential of the proposed model have the same minimum. However, they also agree in a broad neighborhood when $\mathcal{H} = 10$.
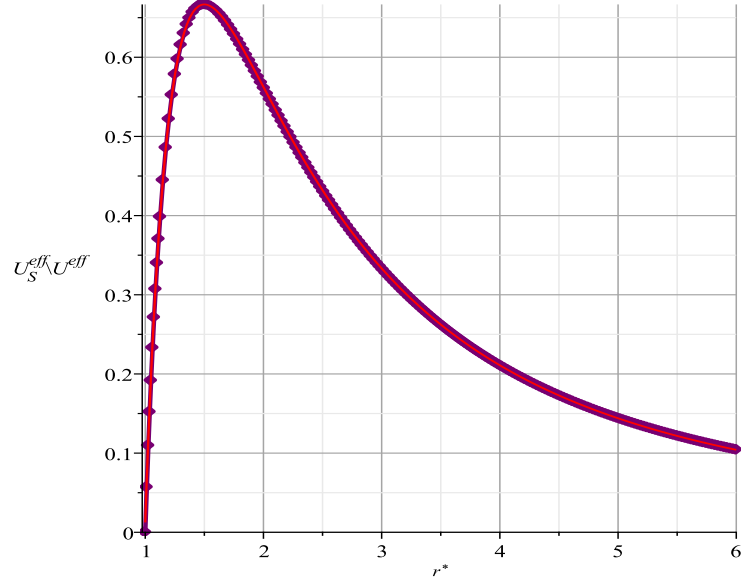
FIG. 4: Diagrammatic scheme of the effective potentials U_S^{eff} (point line) and U^{eff} (solid line) with $\beta = 1$, $\mathscr{L} = 3$ and $\mathcal{H} = 0.1$ for the massless case. It is worth mentioning that for both the BH models the event horizon is located at $r^* = 1$ and the photon sphere for both the potential (U_S^{eff} and U^{eff}) is positioned at $r_\gamma^* = 3/2$.
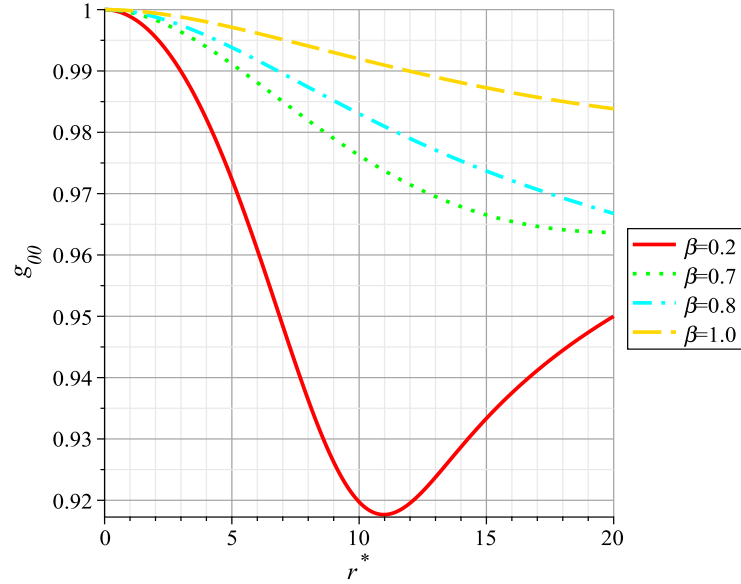

FIG. 5: Behavior of g_{00} versus r^* with $\mathcal{H} = 10$ for various values of β.

V. NON-LOCAL FUZZY SELF-GRAVITATIONAL DIFFUSED DARK MATTER MODELS

By local self-gravitational models, we mean a usual EoS where the radial pressure and energy density are related at a specific point within the fluid distribution, i.e., $p_r(r) = -\rho(r)$. However, the gravitational models where stress-energy tensor constituents do not depend only on the metric, but also functionality extends by taking the average value of energy density throughout the remainder of the distribution, are known as non-local models. Previously, we considered the possibility of developing local self-gravitational anisotropic DM models using a de Sitter-type EoS where the radial pressure has a particular form, $\rho(r) = -p_r(r)$. Using the above-stated conditions, the Einasto parameterization may lead to self-gravitational droplets or regular BH distributions governed by the reformulated mass parameter ω_m. The supposition of non-local EoS with anisotropic fluid configurations has been used in various studies for comprehending the development of compact stellar objects through the mechanism of general relativity
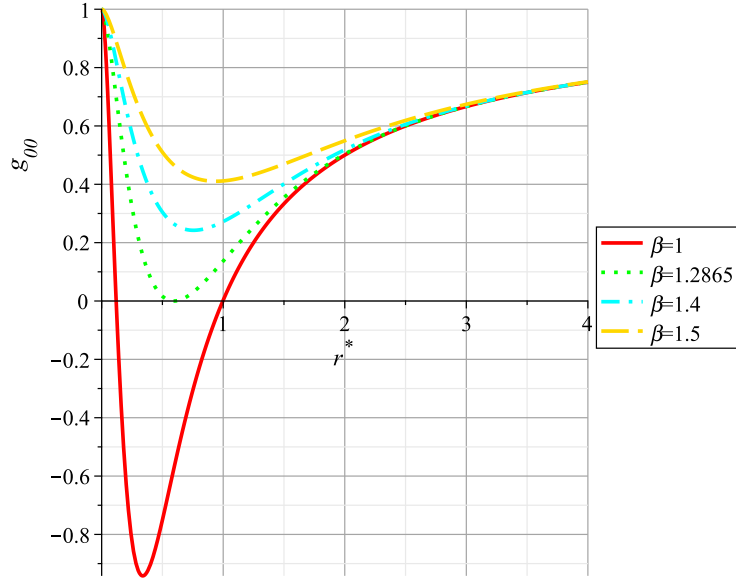
FIG. 6: Behavior of g_{00} versus r^* with $\mathcal{H} = 0.1$ for various values of β. In this case, the event horizon is located at $r^* = 1$, with $\beta = 1$, and is compatible with the standard Schwarzschild BH. However, the extreme BH formed for the case $\beta = 1.2865$ whose event horizon exists at $r_e = 2.33 \times 10^{-7}$pc.
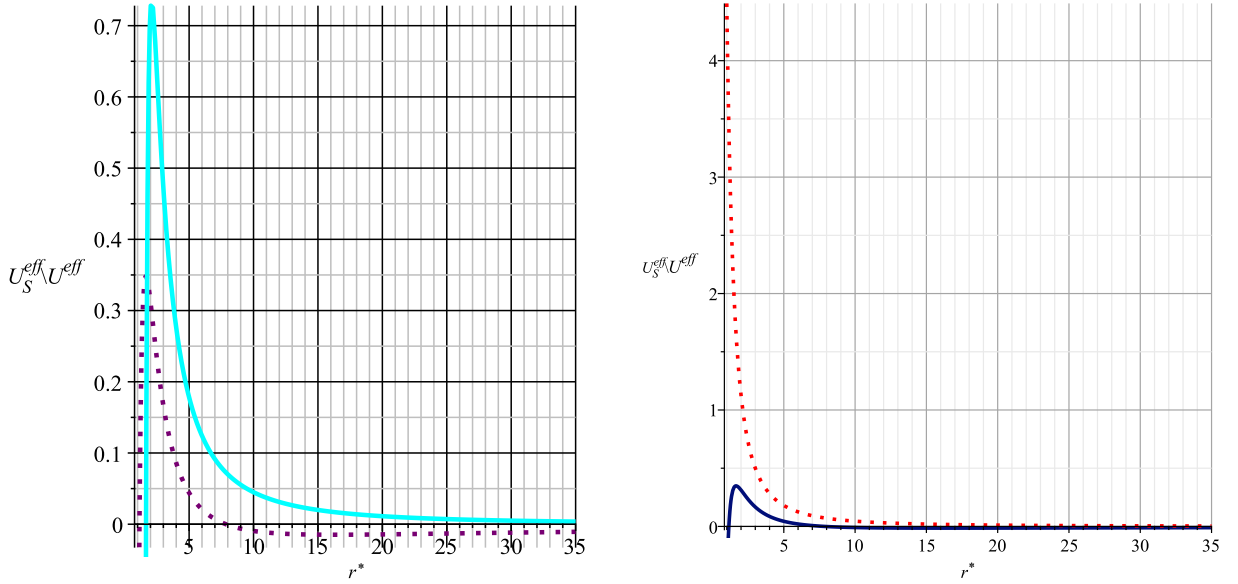

FIG. 7: Behavior of U_S^{eff} (dotted line) and U^{eff} (solid line) versus r^* on the left panel with $\mathcal{H} = 10$, $\mathcal{L} = 3$ and the Einasto index $\beta = 0.2$ for the massive case. Plot of U_S^{eff} (solid line) and U^{eff} (dotted line) versus r^* on the right panel with with $\mathcal{H} = 0.1$, $\mathcal{L} = 3$ and the Einasto index $\beta = 0.1$ for the massive case. The value of he rescaled quantity $\mathcal{H}$ is selected to generate a scaling factor h, comparable in magnitude to the one considered in [51, 52]. Also, $U_S^{\text{eff}}(r_{min}^*) = -0.01477$ and $U^{\text{eff}}(r_{min}^*) = -0.01477$, with $r_{min}^* \approx 16.35$. That is, both the potential (U_S^{eff} and U^{eff}) have a common minimum, and U^{eff} provides a reliable approximation of U^{eff}_S within the neighborhood of r_{min}^*.

[69, 70]. Particularly, we consider an Einasto profile-based charged anisotropic fluid characterized by a non-local EoS whose static limit has the form [71]

$$p_r(r) - \frac{q^2}{8\pi r^4} = \rho(r) + \frac{q^2}{8\pi r^4} - \frac{2}{r^3} \int_0^r x^2 \left(\rho(x) + \frac{q^2}{8\pi r^4} \right) dx. \tag{52}$$
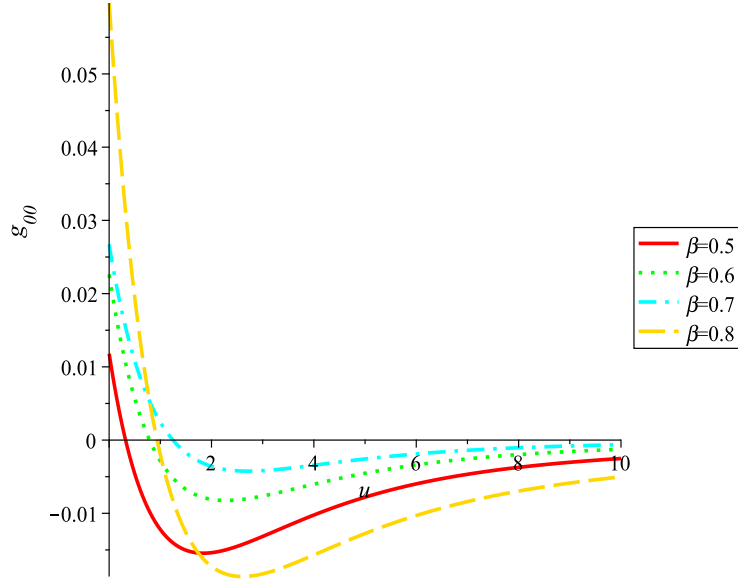
FIG. 8: Diagrammatic scheme of the rescaled form of $\left(p_r - \frac{q^2}{8\pi r^4}\right)\frac{h^2}{\omega}$ against the variable u for various values of β. In the interior region $\left(p_r - \frac{q^2}{8\pi r^4}\right)\frac{h^2}{\omega} > 0$ and vanishes for certain value of u corresponding to the specific selection of parameter β. However, $\left(p_r - \frac{q^2}{8\pi r^4}\right)\frac{h^2}{\omega} < 0$ and displays a minimum beyond the value of u.

This equation signifies the local behavior of $\rho(r)$ and $p_r(r)$. The diffusive behavior of the Einasto density model appears to indicate that non-locality might be important by taking into account the fact that the changes in $\rho(r)$ imply the changes in the $p_r(r)$ through the whole volume. On substituting the density profile (9), the above relation become

$$p_r(r) - \frac{q^2}{8\pi r^4} = \frac{M}{4\pi\Gamma(3\beta)}\left\{\frac{\exp\left[-\left(\frac{r}{h}\right)^{\frac{1}{\beta}}\right]}{3\beta} - \frac{2}{r^3}\gamma\left(3\beta, \left(\frac{r}{h}\right)^{\frac{1}{\beta}}\right)\right\}. \tag{53}$$

We are only concerned with the anisotropic matter distribution at hydrostatic equilibrium. Therefore, the fact that $p_r(r) > 0$ within a region of finite size but $p_r(r) < 0$ outside allows us to present the effective size R of the self-gravitating structure by imposing the constraint $p_r(R) = 0$. Since $\rho \neq 0$ within the region $R < r$, therefore the radius of this type of self-gravitational system will not be finite. We can find R numerically by plotting $p_r(r)h^2$ against $u = \left(\frac{r}{h}\right)^{\frac{1}{\beta}}$. In this respect, let us consider a rescaling of the mass parameter as $\omega = \frac{M}{h}$, thereby Eq. (53) takes the following form

$$\left(p_r - \frac{q^2}{8\pi r^4}\right)\frac{h^2}{\omega} = \frac{M}{4\pi\Gamma(3\beta)}\left[\frac{\exp(-u)}{\beta} - \frac{2}{u^{3\beta}}\gamma(3\beta, u)\right], \tag{54}$$

which by using Eq. (36) turns out to be

$$\left(p_r - \frac{q^2}{8\pi r^4}\right)\frac{h^2}{\omega} = \frac{\exp(-u)}{4\pi}\left[\frac{1}{\beta\Gamma(3\beta)} - 2\sum_{n=0}^{\infty}\frac{u^n}{\Gamma(3\beta + n + 1)}\right]. \tag{55}$$

Furthermore, in FIG. 8, we display the rescaled radial pressure to demonstrate that it is positive within a given region but negative beyond it. However, this does not imply that the gravitational object has a fixed radius because the energy density does not fall to zero outside of this region. In the next step, we examine a configuration of time-independent metric endowed with spherical symmetry coupled with a charged, anisotropic fluid (27) subject to the non-local EoS (52). However, unlike the prior section, we adopt the following ansatz for the metric subject to the Einasto density profile

$$ds^2 = A^2(r)dt^2 - B(r)^{-1}dr^2 - r^2d\Omega^2. \tag{56}$$

Here, it is significant to highlight the fact that $B(r)$ coincides with $g_{rr}(r) = g_{00}^{-1}(r)$ emerging from the metric (10). This immediately suggests that the metric function $B(r)$ will share a similar investigation of the roots of $g_{rr}(r)$ in Sec. as discussed in **III**. Then, the Einstein-Maxwell field equations (16) for this metric yield the following non-zero components

$$\frac{B'}{r} - \frac{1-B}{r^2} = -8\pi\left(\rho + \frac{q^2}{8\pi r^4}\right), \tag{57}$$

$$\frac{2}{r}\frac{A'B}{A} - \frac{1-B}{r^2} = 8\pi\left(p_r - \frac{q^2}{8\pi r^4}\right), \tag{58}$$

$$A'\frac{B}{A} + A''\frac{B}{A} + \frac{B'}{2r} + \frac{A'B'}{2A} = 8\pi\left(p_\perp + \frac{q^2}{8\pi r^4}\right), \tag{59}$$

where primes encode r-derivative. The hydrostatic equilibrium equation for the considered metric (56) is given by

$$p_r' = -(\rho + p_r)\frac{A'}{A} - \frac{2}{r}\left[\frac{q^2}{8\pi r^3}q' - (p_r - p_\perp)\right]. \tag{60}$$

Finally, the integration of Eqs. (57) and (58), respectively provides

$$B(r) = 1 - \frac{2m}{r^2} + \frac{q^2}{r^2}, \tag{61}$$

$$A^2(r) = \exp(\Phi(r)), \quad \Phi(r) = \int \Psi(r)dr \quad \text{with} \quad \Psi(r) = \frac{1}{B}\left[\frac{1}{r}\left(\frac{2m}{r} + \frac{q^2}{r^2}\right) + 8\pi r\left(p_r + \frac{q^2}{8\pi r^4}\right)\right]. \tag{62}$$

In the above relation, the value of the mass function m is provided by (30), whereas the value of $p_\perp$ may be derived from (60) with the help of (62).

$$p_\perp = p_r + \frac{r}{2}\left\{p_r' + \frac{\rho + p_r}{B}\left[\frac{1}{r}\left(\frac{m}{r} - \frac{q^2}{2r^2}\right) + 4\pi r\left(p_r + \frac{q^2}{8\pi r^4}\right)\right] + \frac{2}{r}\left(\frac{q'q^2}{8\pi r^3}\right)\right\}. \tag{63}$$

This expression shows that $B(r)$ is present in the denominator, which shows that $p_\perp$ will turns singular at the roots of $B(r)$. Finally, by using the relation (62), the metric (56) can be transformed in terms of two independent functions $\exp(\Phi(r))$ and $m(r)$ as [31]

$$ds^2 = \exp(\Phi(r))dt^2 - \left(1 - \frac{2m}{r} + \frac{q^2}{r^2}\right)^{-1}dr^2 - r^2d\Omega^2. \tag{64}$$

Here, the functions $\exp(\Phi(r))$ and $m(r)$ are classified as redshift function and shape function, as discussed in [72, 73]. With an anisotropic stress-energy tensor, the above metric fulfills the following wormhole conditions [30].

- The value of tangential pressure $p_\perp(r)$ remains finite, i.e., $p_\perp(r) < \infty$.

- The metric coefficient $B(r)$ has two roots.

The investigation regarding the viability of this type of wormhole can be considered in future projects. We will avoid the later condition by imposing $\omega < \omega_0$, which ensures that the function $\Phi(r)$ is regular everywhere. This condition limits the metric variable $B(r)$ from entering in Eq. (62) and possessing the real zeroes. As a result, we can deduce that the metric (64) outlines a non-local self-gravitational fuzzy DM droplet. By introducing the variable $u = \left(\frac{r}{h}\right)^{\frac{1}{\beta}}$, the expression (63) turns out to be

$$\frac{h^2}{\omega}\left(p_\perp - \frac{q^2}{8\pi r^4}\right) = \frac{1}{4\pi\Gamma(3\beta)}\left[\frac{\gamma(3\beta, u)}{u^{3\beta}} - \frac{u\exp(-u)}{2\beta^2}\right] + \frac{\omega u^{2\beta}}{\Gamma^2(3\beta)\left(1 - \frac{2\omega\gamma(3\beta, u)}{u^\beta\Gamma(3\beta)}\right)}\left[\frac{\gamma(3\beta, u)}{u^{3\beta}} - \frac{\exp(-u)}{\beta}\right]^2. \tag{65}$$
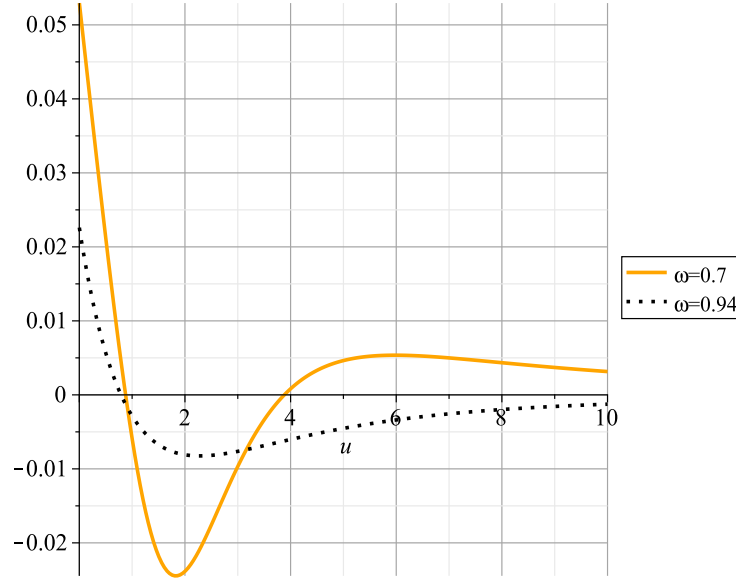
FIG. 10: Pictorial representation of $\frac{h^2}{\omega}\left(p_\perp - \frac{q^2}{8\pi r^4}\right)$ for $\omega = 0.94$ (solid line) and $\frac{h^2}{\omega}\left(p_r - \frac{q^2}{8\pi r^4}\right)$ (dotted line) for $\omega = 0.7$, with $\beta = 1/2$ for different values of the parameter $\omega < \omega_0 = 0.5206$. The above representation has been attained by making use of the expansion formula for the lower incomplete Gamma function given in (36).

FIG. 9: Pictorial representation of the rescaled pressure $\frac{h^2}{\omega}\left(p_\perp - \frac{q^2}{8\pi r^4}\right)$ with Einasto index $\beta = 1/2$ for various values of the parameter $\omega < \omega_0 = 0.5206$. The above representation has been attained by making use of the expansion formula for the lower incomplete Gamma function given in (36).
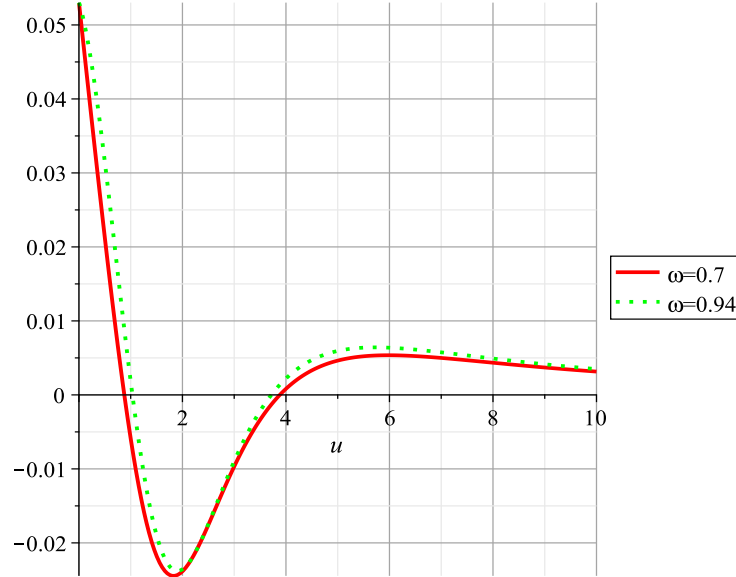
The behavior of rescaled tangential pressure for two different values of the parameter ω is described in FIG. 9. Both curves exhibit negative tangential pressure suggesting the presence of exotic matter, such as that found in self-gravitational compact systems. The tangential pressure diminishes as the distance between curves rises. The parameter ω affects the pressure distribution, with greater values resulting in a flatter profile. In FIG. 10, we plot the rescaled radial and tangential pressures for the same value of β and rescaled mass. It is observed that even for a nonlocal EoS, the self-gravitating droplet does not exhibit any singularity at $r = 0$. This fact can be easily confirmed

by evaluating the Kretschmann scalar $\mathcal{K}$ for the metric (64) as

$$\mathcal{K} = R^{\mu\eta\nu\varsigma}R_{\mu\eta\nu\varsigma} = \frac{2}{r^2}\left(\Psi^2 B^2 + B'^2\right) + \frac{1}{4}\left(\Psi^2 B + 2\Psi' B + \Psi B'\right)^2. \tag{66}$$

The presence of r^{-2} term in this relation does not provide any guarantee that the Kretschmann scalar is singularity-free at $r = 0$ for the assumed Einasto density model. However, by using the expression (36) and taking the limit $r \to 0$, we get

$$\lim_{r \to 0} R^{\mu\eta\nu\varsigma}R_{\mu\eta\nu\varsigma} = \frac{1}{9h^6\beta^4\Gamma^4(3\beta)}[32M^2\beta^2\Gamma^2(3\beta) + \left(2\beta^3 + \beta^2 + \Gamma^2(3\beta) + 2\beta\Gamma^2(3\beta)\right)]. \tag{67}$$

Thus the above expression is singularity-free at $r = 0$. It can be easily shown that at space-like infinity, the metric (64) displays the asymptotic nature at $B(r) \to 1$, whereas the asymptotic nature of the function $\Phi(r)$ can be obtained by using (36) as

$$\Phi(r) = \frac{2\beta M}{(1+\beta)r} + \cdots, \tag{68}$$

where we have neglected the factors that are exponentially decreasing. This implies that the metric (64) is particularized by asymptotically flat manifold because $\exp(\Phi(r)) \to 1$, as $r \to \infty$. This section can be concluded by describing that the compact gravitational droplet enables the bound states of massive particles. Moreover, the effective potential for the spherically symmetric, self-gravitational droplet can be calculated using the formula [68]

$$\mathcal{U}^{\text{eff}}(r) = \frac{\exp(\Phi(r))}{2}\left(\xi + \frac{\ell^2}{r^2}\right), \tag{69}$$

where the terms ℓ and ξ were already specified in Sec. **IV**. By taking into account the fact that the effective potential $\mathcal{U}^{\text{eff}}(r) \geq 0$, we cannot compare this value with the Schwarzschild effective potential. When the total mass M associated with the self-gravitating droplet matches the BH mass M_{BH} at the galactic center, we consider the rescaling as

$$\mathscr{L} = \frac{\ell}{r_s}, \ Q = \frac{q}{r_s}, \ \mathcal{H} = \frac{h}{r_s}, \ r^* = \frac{r}{r_s}, \ \text{with } r_s = 2M_{BH}, \tag{70}$$

then the values of the functions $B(r)$ and $\Phi(r)$ transformed as

$$B(r^*) = 1 + \frac{Q^2}{r^{*2}} - \frac{r^{*2}}{\mathcal{H}^3}\exp\left[-\left(\frac{r^*}{\mathcal{H}}\right)^{\frac{1}{\beta}}\right]f(r^*), \quad \text{where} \quad f(r^*) = \sum_{n=0}^{\infty}\frac{\left(\frac{r^*}{\mathcal{H}}\right)^{\frac{n}{\beta}}}{\Gamma(3\beta + n + 1)}. \tag{71}$$

$$\Phi(r^*) = \frac{1}{\mathcal{H}^3}\int \frac{r^*\exp\left[-\left(\frac{r^*}{\mathcal{H}}\right)^{\frac{1}{\beta}}\right]}{B(r^*)}\left(\frac{2}{\beta\Gamma(3\beta)} + 2\frac{Q^2}{r^{*3}} - 3f(r^*)\right)dr^*. \tag{72}$$

The Einasto density-based self-gravitational model subject to the non-local EoS provided in this section is not captivating for reproducing the galactic motion of S-stars but can be important for the modeling of DM mass coupled with anisotropic fluid allows stabilized trajectories in case of massive particles. Although, this type of self-gravitational droplet is not appropriate for the modeling of central galactic cosmological structures but can be modeled in other galactic areas. Finally, we calculate the values of the physical variables, i.e., the fluid's pressure and the energy density at the center of the gravitational droplet, and compare their values with degenerate matter. Particularly, we take the example of a stellar structure such as a neutron star with degenerate pressure of the order $10^{31} - 10^{34}$ Pa and the usual energy density 10^{17} kg/m^3, however in our case, we assume $M = 10M_\odot$. From the expressions (9) and (52), we have

$$p_r(0) = \frac{c^2}{3}\rho(0), \quad \text{with} \quad \rho(0) = \frac{M}{4\pi h^3\beta\Gamma(3\beta)} \leq \frac{3.387}{4\pi h^3}. \tag{73}$$

In the above relation, we have made use of the fact that the function $1/\beta\Gamma(3\beta)$ exhibit absolute maximum at $\beta = 0.1538$ for $\rho(0)$.

VI. CONCLUSION

This paper examines the effects of the FDM cosmological model on BHs in the presence of electric charge, using a particular density profile proposed by Einasto. This investigation enables us to describe the connection between BH physics and the DM within the background of a spherically symmetric matter distribution. This intriguing correlation between cosmic components interacts with gravitational fields on vast scales and influences the dynamics of galaxies and clusters, leading to new insights. We show that coupling the Einasto density model with an anisotropic stress energy tensor makes it possible to formulate various black hole solutions with specific choices of EoSs. We observed that assuming the EoS $\rho = -p_r$ leads to the formation of a BH solution, which depends on the values of rescaled mass parameter ω or spherically symmetric self-gravitational droplet. We could refer to such an entity as a fuzzy BH if there is no horizon. Although the concept of connecting the galactic centers to the DM is analogous, these DM objects differ from the DM clusters created in [29] their natural composition. Additionally, we have calculated the expression of Hawking temperature for the Einasto-inspired BH solutions within the framework of charged Einstein's gravitational model. For both scenarios, i.e., for fuzzy BH or fuzzy droplet, it is feasible to derive the effective potential that controls the equations of motion. This potential governs the orbits similarly as observed in the case of usual galactic BH. It is noted that the assumption of a non-local EoS rather than a local one gives rise to a self-gravitational droplet. However, in this case, the negative value of p_r appears to be inevitable.

Additionally, this study reveals the existence of an unstable orbit for massive particles with low angular momenta, as well as the formation of bound states. Our analysis also showed that the Einasto density model extends the extension of the Gaussian density profile. Consequently, by considering a more generic formalism the problems relating to the exotic spacetime configuration or perturbative microscopic BH solutions [74] can be addressed under analogous approaches. It is worth mentioning that our conclusions are consistent with the results studied in [75] but by adopting different methods. Specifically, the numerical results presented in [76] demonstrate the presence of DM in the supermassive BH, Sagittarius A^*, composed of "darkinos", as well as a description of the BH through G2 gas clouds.

Data Availability Statement

This manuscript has no associated data or the data will not be deposited. [Authors comment: This manuscript contains no associated data.]

[1] A. R. Brown, D. A. Roberts, L. Susskind, B. Swingle, and Y. Zhao, "Complexity, action, and black holes," *Phys. Rev. D*, vol. 93, p. 086006, 2016.

[2] M. Alishahiha, K. Babaei Velni, and M. R. Mohammadi Mozaffar, "Black hole subregion action and complexity," *Phys. Rev. D*, vol. 99, p. 126016, 2019.

[3] Z. Yousaf, K. Bamba, B. Almutairi, S. Khan, and M. Z. Bhatti, "Role of complexity on the minimal deformation of black holes," *Class. Quantum Grav.*, vol. 41, p. 175001, 2024.

[4] N. Arkani-Hamed, D. P. Finkbeiner, T. R. Slatyer, and N. Weiner, "A theory of dark matter," *Phys. Rev. D*, vol. 79, p. 015014, 2009.

[5] Z. Yousaf, K. Bamba, B. Almutairi, Y. Hashimoto, and S. Khan, "Imprints of dark matter on the structural properties of minimally deformed compact stars," *Phys. Dark Universe*, vol. 46, p. 101629, 2024.

[6] J. B. Jiménez, D. Bettoni, and P. Brax, "Charged dark matter and the h 0 tension," *Phys. Rev. D*, vol. 103, p. 103505, 2021.

[7] M. Vogelsberger, J. Zavala, and A. Loeb, "Subhaloes in self-interacting galactic dark matter haloes," *Mon. Notices Royal Astron. Soc.*, vol. 423, p. 3740, 2012.

[8] J. Zavala, M. Vogelsberger, and M. G. Walker, "Constraining self-interacting dark matter with the milky ways dwarf spheroidals," *Mon. Notices Royal Astron. Soc. Lett.*, vol. 431, p. L20, 2013.

[9] M. Vogelsberger and J. Zavala, "Direct detection of self-interacting dark matter," *Mon. Notices Royal Astron. Soc.*, vol. 430, p. 1722, 2013.

[10] S. Ansoldi, P. Nicolini, A. Smailagic, and E. Spallucci, "Non-commutative geometry inspired charged black holes," *Phys. Lett. B*, vol. 645, p. 261, 2007.

[11] P. Nicolini, A. Smailagic, and E. Spallucci, "Noncommutative geometry inspired schwarzschild black hole," *Phys. Lett. B*, vol. 632, p. 547, 2006.

[12] A. Borde, "Regular black holes and topology change," *Phys. Rev. D*, vol. 55, p. 7615, 1997.

[13] P. R. Brady, "The internal structure of black holes," *Prog. Theor. Phys. Suppl.*, vol. 136, p. 29, 1999.

[14] Y. Nomura, F. Sanches, and S. J. Weinberg, "Black hole interior in quantum gravity," *Phys. Rev. Lett.*, vol. 114, p. 201301, 2015.

[15] C. Bambi, D. Malafarina, and L. Modesto, "Non-singular quantum-inspired gravitational collapse," *Phys. Rev. D*, vol. 88, p. 044009, 2013.

[16] D. Malafarina and P. S. Joshi, "Compact objects from gravitational collapse: an analytical toy model," *Eur. Phys. J. C*, vol. 75, p. 596, 2015.

[17] G. T. Horowitz and J. Maldacena, "The black hole final state," *J. High Energy Phys.*, vol. 2004, p. 008, 2004.

[18] B. Koch, M. Bleicher, and S. Hossenfelder, "Black hole remnants at the lhc," *J. High Energy Phys.*, vol. 2005, p. 053, 2005.

[19] D. Ahn, Y. Moon, R. Mann, and I. Fuentes-Schuller, "The black hole final state for the dirac fields in schwarzschild spacetime," *J. High Energy Phys.*, vol. 2008, p. 062, 2008.

[20] R. Ruffini and J. A. Wheeler, "Introducing the black hole," *Phys. Today*, vol. 24, p. 130, 1971.

[21] M. Heusler, "Black hole uniqueness theorems," 1996.

[22] N. Gürlebeck, "No-hair theorem for black holes in astrophysical environments," *Phys. Rev. Lett.*, vol. 114, p. 151102, 2015.

[23] A. D. Sakharov, "The initial stage of an expanding universe and the appearance of a nonuniform distribution of matter," *Sov. Phys. JETP*, vol. 22, p. 241, 1966.

[24] I. Dymnikova, "Vacuum nonsingular black hole," *Gen. Relativ. Gravit.*, vol. 24, p. 235, 1992.

[25] I. Dymnikova, "The cosmological term as a source of mass," *Class. Quant. Grav.*, vol. 19, p. 725, 2002.

[26] Z. Yousaf, A. Adeel, S. Khan, and M. Z. Bhatti, "Generating fuzzy dark matter droplets," *Chinese J. Phys.*, vol. 88, p. 406, 2024.

[27] S. Khan, A. Adeel, and Z. Yousaf, "Structure of anisotropic fuzzy dark matter black holes," *Eur. Phys. J. C*, vol. 84, p. 572, 2024.

[28] S. Khan and Z. Yousaf, "Construction of fuzzy black holes and self-gravitational droplets in exponential $f(R)$ gravity," *Phys. Scr.*, vol. 99, p. 095304, 2024.

[29] K. Boshkayev and D. Malafarina, "A model for a dark matter core at the galactic centre," *Mon. Not. R. Astron. Soc.*, vol. 484, p. 3325, 2019.

[30] P. Nicolini, "Noncommutative black holes, the final appeal to quantum gravity: a review," *Int. J. Mod. Phys. A*, vol. 24, p. 1229, 2009.

[31] D. Batic, D. A. Abuhejleh, and M. Nowakowski, "Fuzzy dark matter black holes and droplets," *Eur. Phys. J. C*, vol. 81, p. 777, 2021.

[32] D. Batic, J. M. Faraji, and M. Nowakowski, "Possible connection between dark matter and supermassive black holes," *Eur. Phys. J. C*, vol. 82, p. 759, 2022.

[33] P. O. Mazur and E. Mottola, "Gravitational condensate stars," *Proc. Natl. Acad. Sci.*, vol. 101, p. 9545, 2004.

[34] R. Ruffini and S. Bonazzola, "Systems of self-gravitating particles in general relativity and the concept of an equation of state," *Phys. Rev.*, vol. 187, p. 1767, 1969.

[35] A. N. Chowdhury, M. Patil, D. Malafarina, and P. S. Joshi, "Circular geodesics and accretion disks in the Janis-Newman-Winicour and gamma metric spacetimes," *Phys. Rev. D*, vol. 85, p. 104031, 2012.

[36] R. Ruffini, C. R. Argüelles, and J. A. Rueda, "On the core-halo distribution of dark matter in galaxies," *Mon. Notices Royal Astron. Soc.*, vol. 451, p. 622, 2015.

[37] D. Levkov, A. Panin, and I. Tkachev, "Gravitational bose-einstein condensation in the kinetic regime," *Phys. Rev. Lett.*, vol. 121, p. 151301, 2018.

[38] A. Övgün and M. Halilsoy, "Existence of traversable wormholes in the spherical stellar systems," *Astrophys. Space Sci.*, vol. 361, p. 214, 2016.

[39] S. Islam, F. Rahaman, A. Övgün, and M. Halilsoy, "Formation of wormholes by dark matter in the galaxy dragonfly 44," *Can. J. Phys.*, vol. 97, p. 241, 2019.

[40] A. Övgün, "Evolving topologically deformed wormholes supported in the dark matter halo," *Eur. Phys. J. Plus*, vol. 136, p. 987, 2021.

[41] R. C. Pantig and A. Övgün, "Dark matter effect on the weak deflection angle by black holes at the center of milky way and m87 galaxies," *Eur. Phys. J. C*, vol. 82, p. 391, 2022.

[42] A. Övgün, L. J. F. Sese, and R. C. Pantig, "Constraints via eht for black hole solutions with dark matter under the generalized uncertainty principle minimal length scale effect," *arXiv preprint arXiv:2309.07442*, 2023.

[43] R. C. Pantig and A. Övgün, "Dehnen halo effect on a black hole in an ultra-faint dwarf galaxy," *J. Cosmol. Astropart. Phys.*, vol. 2022, p. 056, 2022.

[44] D. Liu, Y. Yang, A. Övgün, Z.-W. Long, and Z. Xu, "Gravitational ringing and superradiant instabilities of the kerr-like black holes in a dark matter halo," *Eur. Phys. J. C*, vol. 83, p. 565, 2023.

[45] R. C. Pantig and A. Övgün, "Black hole in quantum wave dark matter," *Fortschr. Phys.*, vol. 71, p. 2200164, 2023.

[46] Y. Yang, D. Liu, A. Övgün, G. Lambiase, and Z.-W. Long, "Black hole surrounded by the pseudo-isothermal dark matter halo," *arXiv preprint arXiv:2308.05544*, 2023.

[47] E. Retana-Montenegro, E. Van Hese, G. Gentile, M. Baes, and F. Frutos-Alfaro, "Analytical properties of einasto dark matter haloes," *Astron. Astrophys.*, vol. 540, p. A70, 2012.

[48] E. Figueiredo, A. Maselli, and V. Cardoso, "Black holes surrounded by generic dark matter profiles: Appearance and gravitational-wave emission," *Phys. Rev. D*, vol. 107, p. 104033, 2023.

[49] M. Baes, "The einasto model for dark matter haloes," *Astron. Astrophys.*, vol. 667, p. A47, 2022.

[50] J. Einasto, "Kinematics and dynamics of stellar systems," *Trudy Inst. Astrofiz. Alma-Ata*, vol. 51, p. 87, 1965.

[51] J. Einasto, "On galactic descriptive functions," *Astron. Nachr.*, vol. 291, p. 97, 1969.

[52] J. Einasto, "The andromeda galaxy m 31: I. a preliminary model," *Astrophysics*, vol. 5, p. 67, 1969.

[53] J. F. Navarro, E. Hayashi, C. Power, *et al.*, "The inner structure of ΛCDM haloes–III. universality and asymptotic slopes," *Mon. Not. R. Astron. Soc.*, vol. 349, p. 1039, 2004.

[54] V. Springel, S. D. M. White, A. Jenkins, *et al.*, "Simulations of the formation, evolution and clustering of galaxies and quasars," *nature*, vol. 435, p. 629, 2005.

[55] G. A. Mamon and E. L. Lokas, "Dark matter in elliptical galaxies–I. is the total mass density profile of the nfw form or even steeper?," *Mon. Not. R. Astron. Soc.*, vol. 362, p. 95, 2005.

[56] E. Hayashi and S. D. White, "Understanding the halo-mass and galaxy-mass cross-correlation functions," *Mon. Not. R. Astron. Soc*, vol. 388, p. 2, 2008.

[57] L. Gao, J. F. Navarro, S. Cole, C. S. Frenk, S. D. White, V. Springel, A. Jenkins, and A. F. Neto, "The redshift dependence of the structure of massive λ cold dark matter haloes," *Mon. Not. R. Astron. Soc*, vol. 387, p. 536, 2008.

[58] V. F. Cardone, E. Piedipalumbo, and C. Tortora, "Spherical galaxy models with power-law logarithmic slope," *Mon. Not. R. Astron. Soc.*, vol. 358, p. 1325, 2005.

[59] B. K. Dhar and L. L. Williams, "Surface mass density of the einasto family of dark matter haloes: are they sersic-like?," *Mon. Not. R. Astron. Soc.*, vol. 405, p. 340, 2010.

[60] D. Merritt, A. W. Graham, B. Moore, J. Diemand, and B. Terzić, "Empirical models for dark matter halos. i. nonparametric construction of density profiles and comparison with parametric models," *Astron. J*, vol. 132, p. 2685, 2006.

[61] P. F. de Salas, K. Malhan, K. Freese, K. Hattori, and M. Valluri, "On the estimation of the local dark matter density using the rotation curve of the milky way," *J. Cosmol. Astropart. Phys.*, vol. 2019, p. 037, 2019.

[62] D. A. Gadotti, "Structural properties of pseudo-bulges, classical bulges and elliptical galaxies: a sloan digital sky survey perspective," *Mon. Not. R. Astron. Soc.*, vol. 393, p. 1531, 2009.

[63] A. W. Graham and R. Guzmán, "Hst photometry of dwarf elliptical galaxies in coma, and an explanation for the alleged structural dichotomy between dwarf and bright elliptical galaxies," *Astron. J.*, vol. 125, p. 2936, 2003.

[64] V. Springel, J. Wang, *et al.*, "The aquarius project: the subhaloes of galactic haloes," *Mon. Not. R. Astron. Soc.*, vol. 391, p. 1685, 2008.

[65] F. Prym, "Zur theorie der gammafunction.," *J. Reine Agnew. Math.*, vol. 82, p. 165, 1877.

[66] C. M. Urry and P. Padovani, "Unified schemes for radio-loud active galactic nuclei," *Publ. Astron. Soc. Pac.*, vol. 107, p. 803, 1995.

[67] M. Abramowitz and I. A. Stegun, "Handbook of mathematical functions with formulas, graphs, and mathematical tables," *Ninth Dover Printing, Tenth GPO Printing Edition (Dover, New York, 1964).*

[68] T. Fließbach, *Allgemeine Relativitätstheorie*, vol. 3. Springer, 2012.

[69] H. Hernández, L. A. Nunez, and U. Percoco, "Non-local equation of state in general relativistic radiating spheres," *Class. Quantum Grav.*, vol. 16, p. 871, 1999.

[70] H. Abreu, H. Hernández, and L. A. Núñez, "Sound speeds, cracking and the stability of self-gravitating anisotropic compact objects," *Class. Quant. Grav.*, vol. 24, p. 4631, 2007.

[71] H. Hernández and L. A. Núñez, "Nonlocal equation of state in anisotropic static fluid spheres in general relativity," *Can. J. Phys.*, vol. 82, p. 29, 2004.

[72] M. S. Morris and K. S. Thorne, "Wormholes in spacetime and their use for interstellar travel: A tool for teaching general relativity," *Am. J. Phys.*, vol. 56, p. 395, 1988.

[73] M. Visser, "Dirty black holes: Thermodynamics and horizon structure," *Phys. Rev. D*, vol. 46, p. 2445, 1992.

[74] D. Batic, N. G. Kelkar, M. Nowakowski, and K. Redway, "Perturbing microscopic black holes inspired by noncommutativity," *Eur. Phys. J. C*, vol. 79, p. 581, 2019.

[75] E. A. Becerra-Vergara, C. R. Argüelles, A. Krut, J. A. Rueda, and R. Ruffini, "Hinting a dark matter nature of Sgr A* via the S-stars," *Mon. Not. R. Astron. Soc. Lett.*, vol. 505, p. L64, 2021.

[76] J. H. Park *et al.*, "No asymmetric outflows from sagittarius A* during the pericenter passage of the gas cloud G2," *Astron. Astrophys.*, vol. 576, p. L16, 2015.